Compositional structures and thermodynamic properties of Pd-Cu, Rh-Pd, and Rh-Pd-Cu nanoclusters computed by a combined free-energy concentration expansion method and tight-binding approach

Leonid Rubinovich,[1] Michael I. Haftel,[2] Noam Bernstein,[2] and Micha Polak[1]
[1]*Department of Chemistry, Ben-Gurion University, Beer-Sheva 84105, Israel*
[2]*Center for Computational Materials Science, Naval Research Laboratory, Washington, DC 20375-5343, USA*
(Received 31 January 2006; revised manuscript received 17 May 2006; published 7 July 2006)

The statistical-mechanical free-energy concentration expansion method in conjunction with tight-binding elemental bonding energetics are used in atomistic modeling of alloy cluster compositional structures. The study focuses on three systems of 923-atom cuboctahedron clusters, Pd-Cu, Rh-Pd, and Rh-Pd-Cu, each capable of inter-cluster atomic exchange. At low temperatures, cluster core ordering and surface mixed-type ordering are predicted for Pd-Cu compositional "magic-number" clusters, whereas the system of Rh-Pd clusters tends to separate into clusters exhibiting demixed order. In the former case, slight deviations from magic-number compositions strongly affect segregation levels. At high temperatures, Pd-Cu clusters exhibit surface segregation that affects order-disorder transitions, and at even higher temperatures a surface desegregation process, all of which are reflected in characteristic Schottky-type configurational heat capacity versus T curves. Comparing Pd-Cu with Rh-Pd-Cu reveals distinct ternary alloying effects. The role of surface induced bond energy variations in segregation related order-disorder transitions is demonstrated.

DOI: 10.1103/PhysRevB.74.035405 PACS number(s): 61.46.Bc, 68.35.Dv, 82.60.Qr, 36.40.Ei

I. INTRODUCTION

Full atomic-scale chemical-structural information for alloy nanoclusters is desirable for their optimal applicability in technologies based on highly dispersed particles, such as heterogeneous catalysis. In view of limitations in current experimental tools, theoretical modeling, involving a combination of statistical-mechanical approach and input energetics, has been widely employed. There are various theoretical approaches to the cluster energetics, ranging from simplified empirical bond energies[1] or site energies,[2] to somewhat more realistic models, such as the tight-binding (TB) method in the semiempirical second moment approximation.[3–6] More elaborate approaches based on the quantum mechanics of electronic structure such as the TB method[7] and density functional theory (DFT)[8] have been used. Such energetics are used often in conjunction with Monte Carlo or molecular dynamics computer simulations, as well as the genetic algorithm optimization[9,6] for search of global minimum energy. However, time-consuming computer simulations typically provide results for quite limited sets of temperatures and cluster alloy compositions. Simulations based on *ab initio* energetics, such as DFT, are currently feasible for small clusters only.[10]

Other studies employ analytical expressions for the alloy nanocluster free energy based on certain statistical-mechanical approximations. Minimization of the free-energy with respect to atomic site concentrations provides their equilibrium values. In particular, few early works[11,12] used the Bragg-Williams approximation that entirely neglects interatomic correlations (short-range order, SRO). More recently, the free-energy concentration expansion method (FCEM), which is more accurate by including SRO,[13] has proven to be highly efficient in computations of site-specific concentrations versus overall composition, size, and temperature. It provides insight into diverse phenomena and properties specific to alloy clusters, such as mixed and demixed-type compositional order and order-disorder transitions,[14–16] as well as inter-cluster separation and Schottky effects[16,17] in the nanocluster configurational heat capacity. Besides transition metal binary alloy clusters, these studies include temperature dependent properties of ternary clusters, while previous studies focused on zero temperature configurations of alkali metal ternary alloy clusters.[18] However, rather simplistic energetics were used in these FCEM computations involving elemental pair interactions estimated from empirical site energies,[2] with the assumption of equal distribution of the site energy among its nearest neighbor (NN) bonds.[19–22]

The present work studies alloy nanoclusters using FCEM with improved energetics introduced in more detail elsewhere.[23] The basic idea is to incorporate elemental bond energies and their surface-induced variations, obtained by means of the Naval Research Laboratory (NRL) tight-binding method (NRL-TB).[24] The results of this FCEM/NRL-TB approach, applied to surface segregation at flat surfaces ($Rh_{75}Pt_{25}(111)$) as a test case, exhibit good agreement with experiment.[23]

The TB method, developed from the original work by Slater and Koster,[25] can cope with the electronic structure of systems of hundreds of atoms that would otherwise be computationally intractable with *ab initio* techniques such as DFT. Details of the NRL-TB method are described elsewhere.[26–28] The method uses a nonorthogonal TB Hamiltonian, which turns out to be crucial for determining surface energies. The parameters are fit to the augmented plane wave (APW) band structure and equation of state for fcc and bcc structures, and give results in good agreement with APW predictions for most other bulk properties.[27,28] In its original form, the NRL-TB method has been tested in many ways including elastic constants, vacancy formation and stacking fault energies, ductility and thermal expansion, with gener-

ally good agreement with experiment.[27,28] It also performs well for predicting properties of low index faces in *d*-shell fcc metals[24] when charge self-consistency is included in the calculations. In particular, calculated nearest neighbor bond energies in bulk and surface environments, used in the present work, largely account for trends in surface energies and interlayer relaxations.[24] This fact is expected to be sufficient for NRL-TB to work for the rather large clusters treated in this study. Moreover, there is some evidence that it also works well and gives results similar to DFT even for some undercoordinated systems, namely thin metal nanowires.[29–31] It can be noted that energies computed with the tight-binding approach implicitly include some many-body effects. The accuracy of the predictions can be further improved by explicitly adding many-body contributions to the TB matrix elements.[32] The role of many-body effects in certain alloy properties was recently demonstrated by the cluster expansion method.[33]

According to previous studies, the structure of free metal clusters can alter depending on size and obey the tendency to form energy-minimizing perfect compact shapes that consist of "geometrical magic numbers" of atoms.[10] While relatively large free clusters possess internal structures corresponding to the bulk lattice symmetry in the macroscopic limit, such as cuboctahedron (CO_h) in fcc metals, smaller particles can undergo morphological transitions to icosahedron (I_h) driven by the tendency to diminish surface energy and accompanied by emergence of internal strain.[4] The crossover size depends strongly on the metal, and is controlled by the range of the interatomic potential.[4,34] The present computations focus mainly on medium size 923-atom clusters, which were predicted for Pd and Rh to have the cuboctahedron shape (TB calculations[7]).

II. FCEM/NRL-TB METHOD ADAPTED TO CLUSTERS

The FCEM expression for the free energy of multicomponent alloy clusters, obtained using nearest neighbor (NN) pair-interaction model Hamiltonian and expansion in powers of constituent concentrations, is given by:[16]

$$F = kT\sum_p \left(N_p \sum_I c_p^I \ln c_p^I \right) + \sum_{p\leqslant q} N_{pq} \left\{ \frac{1}{2}\sum_I w_{pq}^{II}(c_p^I + c_q^I) - \sum_{\{IJ\}} \left[V_{pq}^{IJ}(c_p^I c_q^J + c_p^J c_q^I) + kTc_p^I c_p^J c_q^I c_q^J \frac{1}{b} \ln\left(\cosh\left(b\frac{2V_{pq}^{IJ}}{kT} \right) \right) \right] \right\}.$$

When applied to clusters consisting of atoms located at centro-symmetric concentric "shells," numerical minimization of F yields all I-constituent equilibrium concentrations for shell number p, c_p^I. Geometric input parameters include the number of atoms in each shell, N_p, and the number of NN pairs belonging to p and q shells, N_{pq}. The first term contributes to the configurational entropy, the second term involves the elemental (homoatomic) interactions, w_{pq}^{II}, the third term includes the effective heteroatomic interactions, V_{pq}^{IJ}, between constituents I and J $\left[V_{mn}^{IJ}=\frac{1}{2}(w_{mn}^{II}+w_{mn}^{JJ}-2w_{mn}^{IJ})\right]$, and the last term in F involves short-range order contributions ($b\approx 0.6$ is a constant obtained from a best fit of FCEM predictions to Monte Carlo simulations[16]).

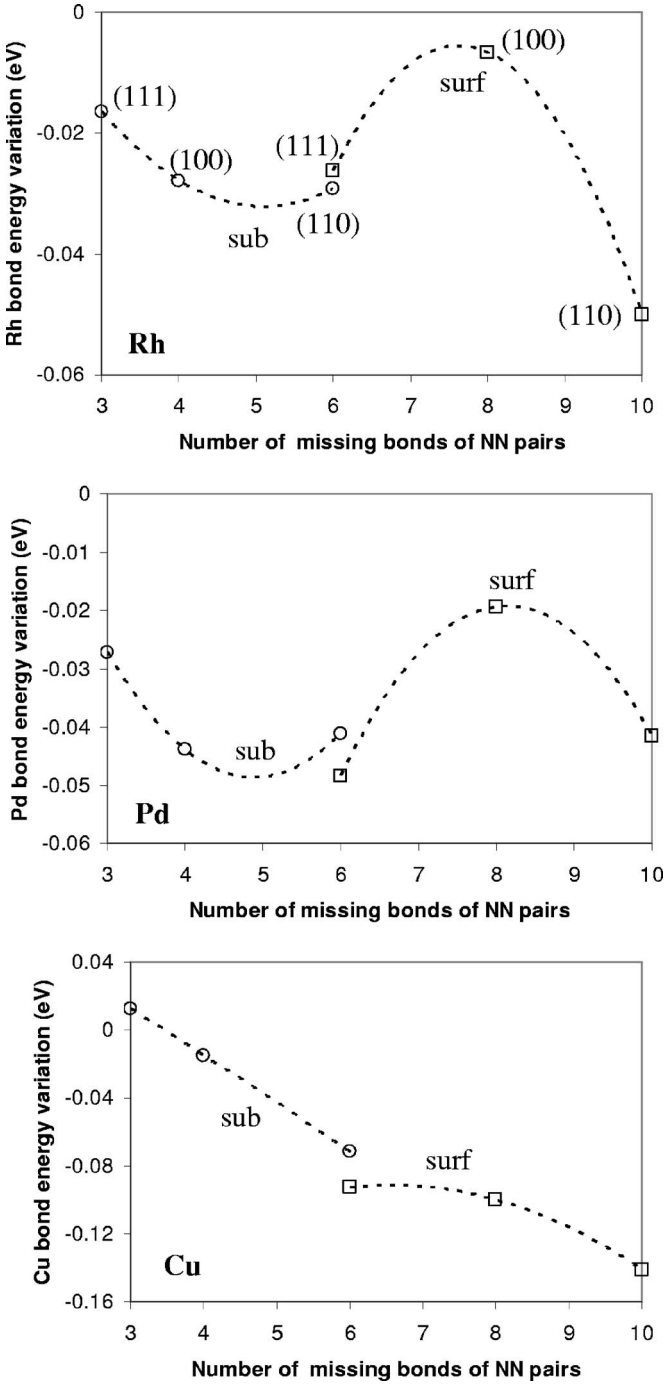

FIG. 1. NRL-TB computed variations of elemental bond energy, $\delta w_{pq}^{II}=w_{pq}^{II}-w_{bulk}^{II}$, for the three low-index surface orientations. sub =surface/subsurface bonds, surf=surface/surface bonds. Dashed lines are parabolic fits.

Figure 1 presents NRL-TB data concerning variations, δw_{pq}^{II}, of surface-surface (surf) and surface-subsurface (sub) elemental bond energies $w_{pq}^{II}(=w_{\text{bulk}}^{II}+\delta w_{pq}^{II})$ for different surface orientations[24] versus the number of missing bonds of

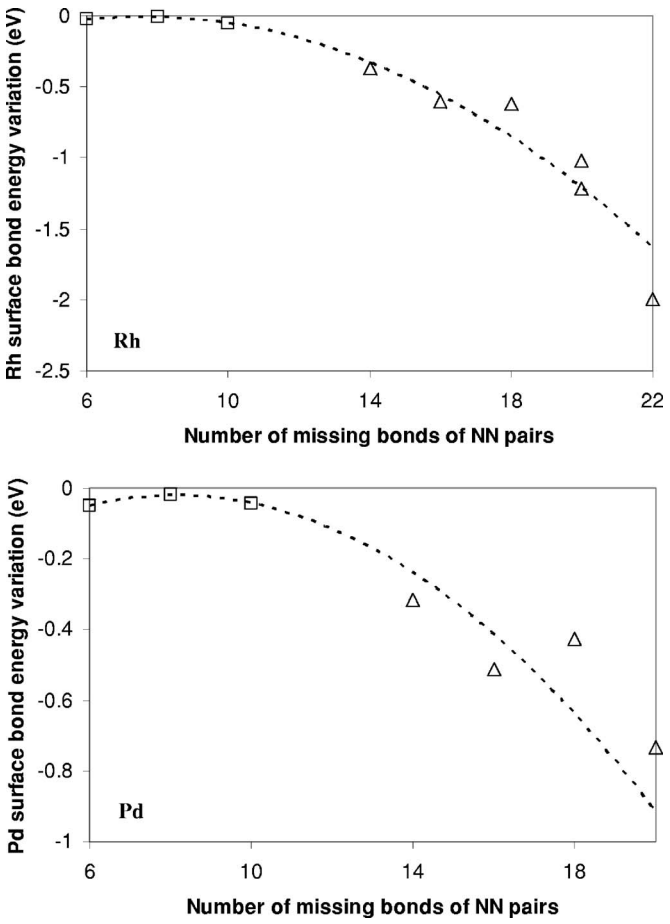

FIG. 2. Variations of surface/surface bond energies extending from the planar surfaces shown in Fig. 1 (squares) to surfaces of very small clusters (Refs. 35 and 36) (including Rh dimer having 22 missing bonds as compared to inner bond in the fcc structure). The latter variations are denoted by triangles, and the dashed lines represent the same parabolic fits as in Fig. 1.

NN pairs. Interpolation and extrapolation of these data provide bond energies for other coordinations relevant to cluster surfaces. Notably, extrapolating the parabolic fit of the NRL-TB data (surf) for flat surfaces to lower coordinations reproduces well the bond variations obtained by us using TB data for elemental cluster energies as computed by Barreteau *et al.*[35,36] (Fig. 2). Contributions of elemental bond energies to the FCEM expression can also be given by site-specific surface and subsurface tensions.[23] General segregation trends in this system can be inferred from TB calculations,[24] yielding $\gamma^{\mathrm{Cu}} < \gamma^{\mathrm{Pd}} < \gamma^{\mathrm{Rh}}$. Experimental heats of mixing indicate separation tendencies in Rh-Pd[37] and Rh-Cu[2] with effective interactions $V^{\mathrm{RhPd}} = -35$ meV and $V^{\mathrm{RhCu}} = -23$ meV, and ordering tendency in Pd-Cu[38] with $V^{\mathrm{PdCu}} = 33$ meV, all derived by the FCEM formula of Ref. 39, that relates V_{pq}^{IJ} to ΔH^{mix} (the heteroatomic interactions, w_{pq}^{IJ}, can be estimated using V_{pq}^{IJ} and the tight-binding computed elemental interactions, w_{pq}^{II} and w_{pq}^{JJ}, but do not appear explicitly in F).

Taking into account that the atomic radii of Pd and Cu differ by ~7%, possible atomic size mismatch (SM) effects can somewhat modify surface segregation, although it was argued that in alloy nanoclusters a rather small effect is generally expected, except in case a very large size mismatch (e.g., ~14% for Ni-Ag or for Ni-Au).[2] Otherwise, relaxations of the cluster structure (as compared to that of the alloy bulk) as well as finite matter effects might diminish SM contributions to segregation. Since Rh and Pd have rather similar atomic radii, with only about ~2% difference (Rh and Cu differ by ~5%), SM is less important in Rh-Pd clusters. In Rh-Pd-Cu clusters small SM effects are expected, for overall concentrations and temperatures with complete Cu surface segregation.

Substitution of computed sets of constituent shell concentrations in the FCEM expression provides the temperature dependent free energy. Then, according to common expressions, other thermodynamic functions, including the cluster configurational heat capacity, can be readily calculated.

III. COMPUTATION PROCEDURE AND RESULTS

The free energy was minimized with respect to the number of independent variables (shell or site concentrations), which for 923-atom cuboctahedrons with 36 shells around a central atom, is equal to 36 and 72 for binary and ternary alloys, respectively. The search for the global minimum in the "concentration landscape" was done with the MATLAB computation package in 20 K temperature steps. The procedure of constrained minimization (using the "fmincon" function) is quite straightforward at high temperatures due to dominant, relatively smooth entropy contributions and to the proximity of the minimum to a random atomic distribution. At lower temperatures, a complex energetics related landscape can result in sharp changes in shell concentrations ("phase transitions"), and therefore the genetic algorithm was employed to verify the general position of the global minimum. A subsequent run of "fmincon" as a hybrid function finally specified the accurate position of the minimum, namely yielding equilibrium site concentrations.

The 923-atom cuboctahedrons exhibit at low temperatures a variety of compositional structures with mixed or demixed-type order, depending on the nature of the elemental/effective interactions and the overall constituent concentrations. Only part of the results is presented here exemplifying some characteristic phenomena such as the interplay of order, disorder and surface segregation, as well as pertinent configurational heat capacity.

Cu-Pd. Starting with binary clusters, Cu-Pd 923-atom clusters with increasing Cu overall concentration exhibit competitive multi-site segregation (Fig. 3). Since Cu atoms have weaker bonding, they tend to populate lower coordinated sites, so that as Cu content increases it substitutes Pd sequentially at vertexes, edges, (100) and (111) faces. Moreover, attractive Pd-Cu effective interactions cause a sequence of ordered compositional structures indicated by flat regions in the 100 K curves. Starting with complete vertex site occupation, up to ~0.24 overall Cu concentration all Cu atoms segregate at the surface, thereby facilitating mixed order that involves edges and then faces over a pure Pd core (Fig. 3). At higher Cu contents $L1_2$-like ordered structure develops starting from the cluster core center below the ordered sur-

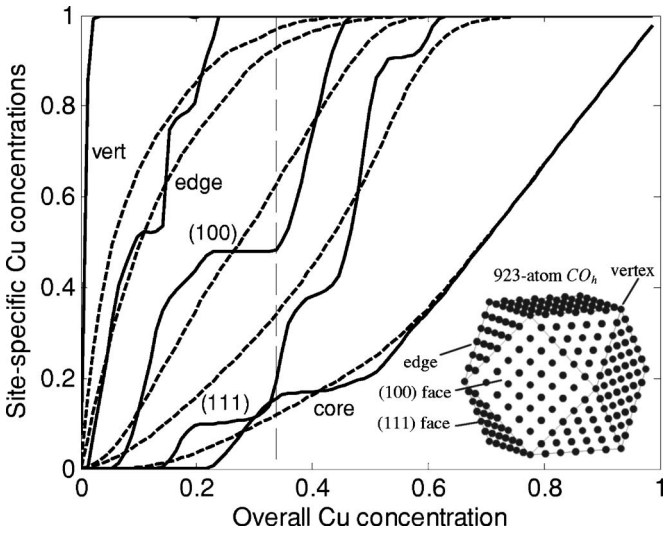

FIG. 3. Sequential multi-site segregation of copper computed by the FCEM/NRL-TB method for $Pd_{1-x}Cu_x$ 923-atom CO_h clusters (100 K-solid lines, 500 K-dashed lines). The compositional magic-number fully ordered structure $Pd_{618/923}Cu_{305/923}$ [structure I, depicted in Fig. 4(a)] is indicated by the vertical dashed line.

face, until full order is predicted for a "magic-number" composition $Pd_{618/923}Cu_{305/923}$ [structure I, Fig. 4(a)]. It should be noted that the global minimum of the free energy corresponding to the stable structure I is only slightly deeper than a local minimum related to a metastable similar structure (II) with "anti-phase" (100) order and a slightly different overall composition, $Pd_{612/923}Cu_{311/923}$ [Fig. 4(b)]. (As described below, structure II is the stable configuration when simple bond breaking energetics are used.) The predicted $L1_2$-type order in Pd-Cu CO_h is consistent with results of Mottet *et al.*,[3] obtained by Monte Carlo simulations for an energetic model based on semi-empirical pair or many-body potentials, derived from the electronic structure of alloys. The multi-site competition, $L1_2$-type core and mixed surface order, based here on improved input energetics, are in qualitative agreement with our previous results for smaller 309-atom CO_h.[14] Off-stoichiometry effects are responsible for the steep rises in Cu segregation beyond the flat regions, similarly to effects

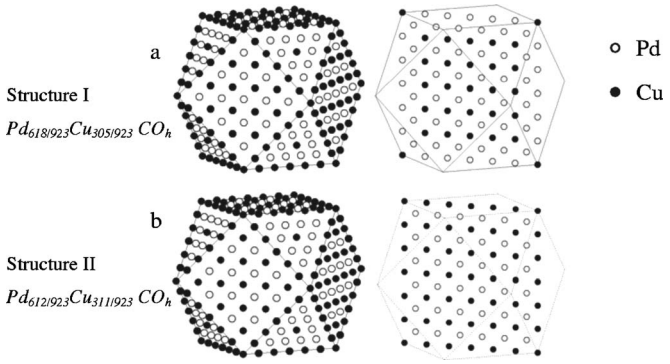

FIG. 4. (a) Outline of structure I with surface "mixed" order (left) and cross section of the $L1_2$-like ordered core (right) predicted for low temperatures. (b) An alternative structure II with anti-phase (100) order, corresponding to simple bond-breaking energetics.

predicted by us previously[40] and by Ruban[41] for cases of bulk intermetallic alloys. Below the magic-number composition $Pd_{618/923}Cu_{305/923}$ the tendency to preserve the ordered surface forces the extra Cu atoms to move into the core. When core order is established, face concentrations start to grow again sharply, and correspondingly the surface order disappears. All order/disorder related segregation features vanish at 500 K, while the site occupation sequence (from vertex to core) is preserved.

The temperature evolution of the sublattice and overall concentrations computed for the (100) and core in the $Pd_{618/923}Cu_{305/923}$ compositional structure are shown in Fig. 5(a). With temperature increase, a sequence of disordering processes involving the (111) faces (not shown), core and then the (100) faces, follows the expected trend of more stable order in alloys having higher solute concentration. In addition, in the course of disordering the (100) face Cu segregation increases up to a maximum associated with the interplay of surface segregation and atomic order[13] [Fig. 5(a)]. Correspondingly, a remarkable multi-peak heat capacity curve that exhibits four Schottky-type features,[16,17] is related to the order-disorder transitions at the faces and core and subsequent Cu desegregation [Fig. 5(c)].

It is instructive to compare the TB computed low temperature structure and its temperature evolution with those computed by means of a simple bond breaking model (SBBM), in which the interactions entering the free-energy equation are considered as coordination independent constants, i.e., no surface induced bond energy variations are assumed. The comparison reveals prominent differences as follows. For $Pd_{618/923}Cu_{305/923}$ as well as $Pd_{612/923}Cu_{311/923}$ the TB more intense strengthening of Cu surface bonds compared to Pd (Fig. 1), stabilizes structure I [Fig. 4(a)], while SBBM predicts structure II as the stable one (Fig. 4(b); for both energetics the six atom deviation from the stoichiometric magic number compositions causes only slight changes in the corresponding structures). In the SBBM computations both the core and surface order-disorder transitions appear at higher temperatures than with TB energetics [e.g., Fig. 5(b) vs Fig. 5(a) for $Pd_{618/923}Cu_{305/923}$], and these shifts are reflected distinctly in the respective heat capacity curves [Fig. 5(d) vs Fig. 5(c)]. Thus, the more intense strengthening of Cu surface bonds enhances its segregation at the cluster surface (accompanied by higher core depletion), which are at the origin of disordering and the reduced order-disorder transition temperatures. Furthermore, the well-resolved surface and core heat capacity features obtained in the TB computations, compared to partial overlap of the SBBM computed features [Fig. 5(d) vs Fig. 5(c)] are clearly associated with the strengthening of surface and subsurface bond energies relative to the core bonding.

Rh-Pd. Due to repulsive effective interactions, binary clusters can exhibit surface-core segregation/separation or surface demixed order[15] at definite magic number overall compositions. Moreover, in a system of clusters capable of atomic exchange, the derived sets of shell concentrations can be considered as true equilibrium values only after evaluation of the mixing free energy, defined as the difference between the alloy and the pure element cluster free energies.[14] Inspection of the shape of the mixing free-energy versus

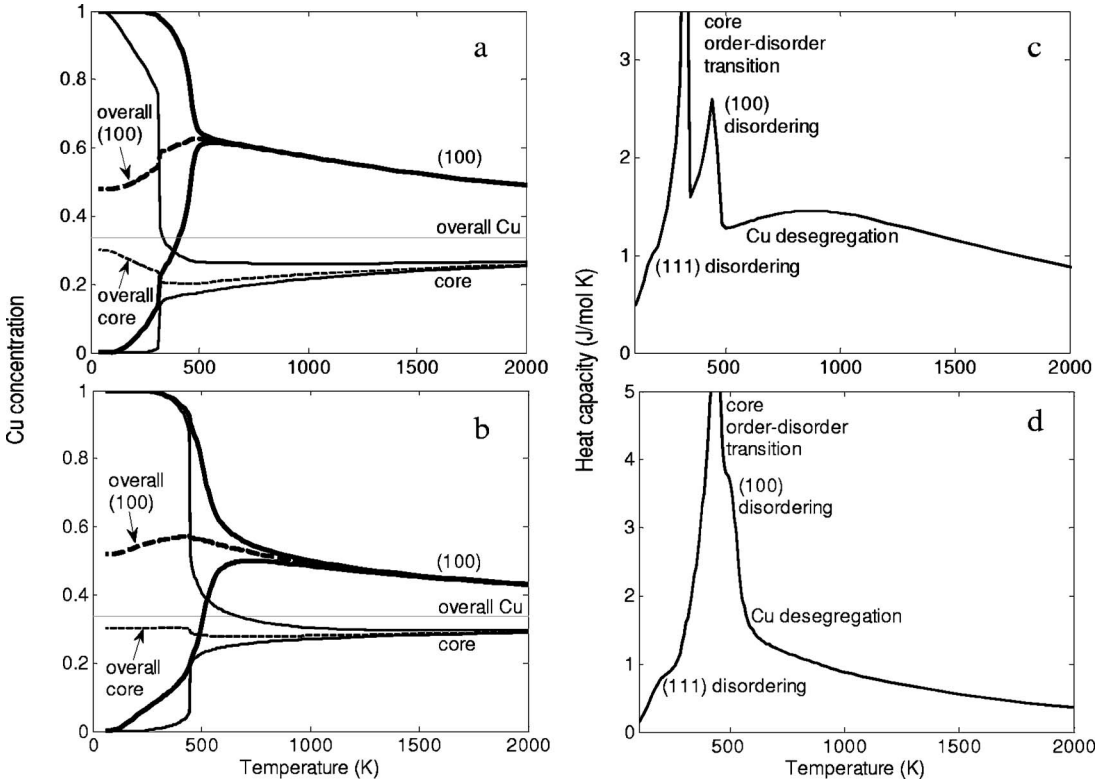

FIG. 5. Order-disorder transitions and segregation/desegregation in magic number $Pd_{618/923}Cu_{305/923}$ CO_h clusters. Computations based on NRL-TB energetics: (a) The solid lines depict the (100) and core Cu concentrations vs T at Cu and Pd sublattices [denoted in Fig. 4(a) by solid and open circles, respectively]. Dashed lines depict the overall (100) and core Cu concentrations; (c) The overall configurational heat capacity curve exhibiting Schottky-type features. Corresponding computations for the same compositional magic number assuming no bond energy variations at surface sites (SBBM, $\delta w_{pq}^{II}=0$) are given in (b) and (d), respectively.

overall concentration curve reveals that the effective repulsion can be manifested in convexity reflecting inter-cluster "phase" separation between two magic-number structures. These phenomena were predicted by us previously for 13–55 atom Rh-Ni-Cu clusters and the corresponding binary alloy systems using empirical energetics.[16,17] Since for 923-atom clusters the number of magic-number structures is large, the convex concentration regions of separation become correspondingly narrow and less pronounced, so we have chosen to focus on the 147-atom Rh-Pd CO_h cluster using the NRL-TB energetics (Fig. 6). At 10 K the curve exhibits four regions of convexity, each ranging between two stable structures: (i) pure Pd, (ii) Rh inclusion comprising part of the core, (iii) entire Rh core, (iv) Rh (100)+entire core, and (v) Rh cluster with Pd vertexes (see schematics from left to right in Fig. 6). Around 500 K almost all the convexities disappear [except the one between (i) and (ii)], indicating stabilization of one-type clusters having intermediate concentrations.

Rh-Pd-Cu. In this system, since bond and surface energies of the constituents decrease strongly from Rh to Pd and Cu, Rh is expected to populate cluster core sites, while Cu (and perhaps Pd) should populate surface sites. We have chosen to compute the temperature evolution of the compositional structure of the $Rh_{561/923}Pd_{150/923}Cu_{212/923}$ magic-number cluster. At low temperatures, it has a pure Rh core and exhibits the same type of surface order as discussed above for the $Pd_{618/923}Cu_{305/923}$ binary cluster [structure I, Fig. 4(a)]. Variations in the overall Cu concentration at the (100) face, together with concentrations of the corresponding sublattices, compared to the binary cluster, are shown in Fig. 7, top. While core disordering in the binary cluster is associated

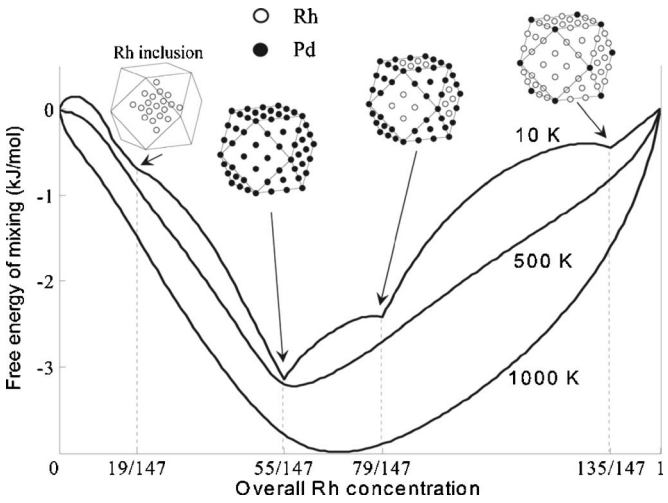

FIG. 6. Mixing free energies computed for Rh-Pd 147-CO_h clusters equilibrated at three temperatures. Convexities between magic-number compositional structures (shown schematically) indicate inter-cluster separation concentration regions. (The 128 Pd outer atoms in the 19/147 structure are not shown.)

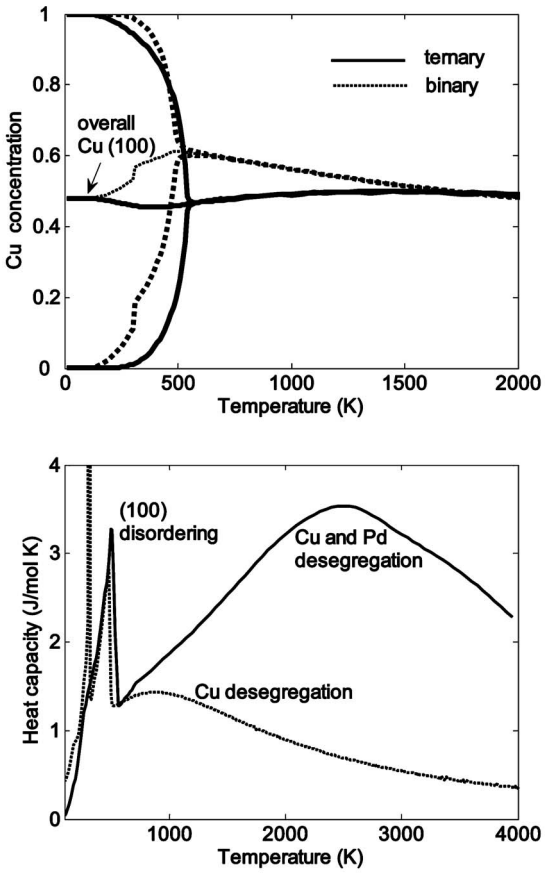

FIG. 7. Surface order-disorder transitions and desegregation in magic number $Rh_{561/923}Pd_{150/923}Cu_{212/923}CO_h$ clusters. Dashed lines correspond to the binary $Pd_{618/923}Cu_{305/923}$ clusters. Top: (100) Cu concentrations at Cu and Pd sublattices. Bottom: The overall configurational heat capacity curve. Note that a core-disordering peak appears only in the binary case.

with Cu surface segregation and a corresponding deviation of surface composition from stoichiometry, in the ternary cluster, due to the strong Rh-Rh bonding, the overall core and surface compositions remain nearly unaltered in the phase transition region. This difference seems to be the main origin of a ~50 K shift upwards (relative to the binary case) in the corresponding heat capacity peak (Fig. 7, bottom). Moreover, in spite of the attractive effective interactions between Pd and Cu, as compared to effective Rh-Cu repulsion, the estimated interaction between Cu and the Rh core atoms is slightly stronger than with the Pd atoms. Possibly, this is an additional contribution to the relative stabilization of surface order in the ternary cluster, and both factors can be termed "substrate (core) effects."

Compared to the Cu desegregation heat capacity feature in the binary cluster (Fig. 7, bottom), in the ternary case the broader peak is centered higher, at around 2500 K, reflecting the much higher segregation driving force associated with the strong Rh-Rh bonding. These Cu and Pd desegregation processes occur only at high temperatures, while for lower temperatures the neglect of size mismatch effects is justified since the atomic disordering exchange occurs mainly within the Pd-Cu surface/crust over the Rh core. Finally, in the binary case the desegregation heat capacity peak is much less intense (Fig. 7, bottom) because Cu atoms are present also in the core (and Pd atoms also at the surface) even at low temperatures, thereby diminishing the number of available surface-core desegregation excitations.[17]

IV. CONCLUSIONS

The combination of the statistical-mechanical FCEM with energetics based on the NRL-TB method was applied to alloy clusters. It revealed for Rh-Pd-Cu, Rh-Pd, and Pd-Cu 923-atom CO_h compositional structures and thermodynamic properties, controlled by relative elemental bond strengths decreasing from Rh to Pd and Cu, and by Rh-Pd, Rh-Cu repulsive, and Pd-Cu attractive effective interactions. Compared to empirical energetics used before, the choice of tight-binding data concerning surface-induced bond energy variations is expected to improve the accuracy of the computations, which show at low temperatures: (1) Core and segregated-surface mixed order in Cu-Pd clusters; (2) Rh-Pd-Cu clusters with mixed surface order over pure Rh core; and (3) Rh-Pd clusters separated into magic-number compositional structures exhibiting demixed order.

At higher temperatures, disordering transitions and desegregation are reflected as Schottky-type peaks in the configurational heat capacity versus T, which appears to be most illuminating when such thermal processes are concerned. Distinct strengthening of surface bonds affects segregation that destabilizes ordered structures.

While in the present study elemental bond energies relevant mostly to 923-atom cluster surfaces were estimated by interpolation and extrapolation procedures based on TB data of flat surface with different orientations, it seems desirable, especially for smaller clusters, to obtain data concerning elemental (as well as heteroatomic) bond energy variations by direct TB electronic structure computations. Inclusion of next-nearest neighbor and explicit many-body interaction terms can improve the accuracy of the FCEM results.

ACKNOWLEDGMENT

This research was supported by The Israel Science Foundation (Grant No. 1204/04).

[1] V. S. Sundaram and P. Wynblatt, Surf. Sci. **52**, 569 (1975).
[2] L. Zhu and A. E. DePristo, J. Catal. **167**, 400 (1997).
[3] C. Mottet, G. Treglia, and B. Legrand, Phys. Rev. B **66**, 045413 (2002).
[4] F. Baletto, R. Ferrando, A. Fortunelli, F. Montalenti, and C. Mottet, J. Chem. Phys. **116**, 3856 (2002).
[5] S. Darby, T. V. Mortimer-Jones, R. L. Johnston, and C. Roberts, J. Chem. Phys. **116**, 1536 (2002).
[6] L. Johnston, J. Chem. Soc. Dalton Trans. **22**, 4193 (2003).
[7] C. Barreteau, M. C. Desjonqueres, and D. Spanjaard, Eur. Phys. J. D **11**, 395 (2000).
[8] E. Apra, F. Baletto, R. Ferrando, and A. Fortunelli, Phys. Rev. Lett. **93**, 065502 (2004).
[9] F. Baletto, C. Mottet, A. Rapallo, G. Rossi, and R. Ferrando, Surf. Sci. **566**, 192 (2004).
[10] F. Baletto and R. Ferrando, Rev. Mod. Phys. **77**, 371 (2005).
[11] J. M. Montejano-Carrizales and J. L. Moran-Lopez, Surf. Sci. **239**, 169 (1990).
[12] J. M. Montejano-Carrizales and J. L. Moran-Lopez, Surf. Sci. **239**, 178 (1990).
[13] M. Polak and L. Rubinovich, Surf. Sci. Rep. **38**, 127 (2000).
[14] L. Rubinovich and M. Polak, Phys. Rev. B **69**, 155405 (2004).
[15] M. Polak and L. Rubinovich, Int. J. Nanosci. **3**, 625 (2004).
[16] M. Polak and L. Rubinovich, Surf. Sci. **584**, 41 (2005).
[17] M. Polak and L. Rubinovich, Phys. Rev. B **71**, 125426 (2005).
[18] A. Bol, J. A. Alonso, J. M. Lopez, and A. Mananes, Z. Phys. D: At., Mol. Clusters **30**, 349 (1994).
[19] R. L. Schwoebel, J. Appl. Phys. **38**, 3154 (1967).
[20] R. G. Donnelly and T. S. King, Surf. Sci. **74**, 89 (1978).
[21] T. S. King and R. G. Donnelly, Surf. Sci. **141**, 417 (1984).
[22] J. K. Strohl and T. S. King, J. Catal. **116**, 540 (1989).
[23] M. Polak and L. Rubinovich (unpublished).
[24] M. I. Haftel, N. Bernstein, M. J. Mehl, and D. A. Papaconstantopoulos, Phys. Rev. B **70**, 125419 (2004).
[25] J. C. Slater and G. F. Koster, Phys. Rev. **94**, 1498 (1954).
[26] R. E. Cohen, M. J. Mehl, and D. A. Papaconstantopoulos, Phys. Rev. B **50**, 14694 (1994).
[27] M. J. Mehl and D. A. Papaconstantopoulos, Phys. Rev. B **54**, 4519 (1996).
[28] D. A. Papaconstantopoulos and M. J. Mehl, J. Phys.: Condens. Matter **15**, R413 (2003).
[29] F. D. Novaes, A. J. R. da Silva, E. Z. da Silva, and A. Fazzio, Phys. Rev. Lett. **90**, 036101 (2003).
[30] E. Z. da Silva, A. J. R. da Silva, and A. Fazzio, Phys. Rev. Lett. **87**, 256102 (2001).
[31] K. Gall, J. Diao, M. L. Dunn, M. Haftel, N. Bernstein, and M. J. Mehl, J. Eng. Mater. Technol. **127**, 417 (2005).
[32] G. Staszewska, P. Staszewski, N. E. Schultz, and D. G. Truhlar, Phys. Rev. B **71**, 045423 (2005).
[33] V. Blum and A. Zunger, Phys. Rev. B **69**, 020103(R) (2004).
[34] J. P. K. Doye, D. J. Wales, and R. S. Berry, J. Chem. Phys. **103**, 4234 (1995).
[35] C. Barreteau, D. Spanjaard, and M. C. Desjonqueres, Phys. Rev. B **58**, 9721 (1998).
[36] C. Barreteau, D. Spanjaard, and M. C. Desjonqueres, Surf. Sci. **433**, 751 (1999).
[37] K. M. Myles, Trans. Metall. Soc. AIME **242**, 1523 (1968).
[38] O. Kubaschewski and C. B. Alcock, *Metallurgical Thermochemistry* (Pergamon, Oxford, 1979).
[39] L. Rubinovich and M. Polak, Surf. Sci. **513**, 119 (2002).
[40] M. Polak and L. Rubinovich, in *Alloy Surface Segregation and Ordering Phenomena: Recent Progress*, edited by D. P. Woodruff, *Surface Alloys and Alloy Surfaces, The Chemical Physics of Solid Surfaces* (Elsevier Science, Amsterdam, 2002), Vol. 10, pp. 86–117.
[41] A. V. Ruban, Phys. Rev. B **65**, 174201 (2002).